Fractal basin boundaries in coupled map lattices

Ying-Cheng Lai* and Raimind L. Winslow
Department of Biomedical Engineering, The Johns Hopkins University School of Medicine, Baltimore, Maryland 21205
(Received 21 January 1994)

It has been suggested that spatiotemporal dynamical systems cannot exhibit fractal basin boundaries, as interactions among chaotic elements at different spatial sites may destroy fine scale phase-space structures. We present evidence of an extreme type of fractal basin boundary in spatiotemporal chaotic systems modeled by globally coupled, two-dimensional maps. The existence of fractal basin boundaries for these systems indicates an extreme sensitive dependence of asymptotic attractors on both initial conditions and parameters.

PACS number(s): 05.45.+b

Fractal basin boundaries are ubiquitous in low-dimensional nonlinear dynamical systems that exhibit multiple attractors [1,2]. For such systems, basins of attraction are separated by fractal sets called fractal basin boundaries. It is impossible to predict, with certainty, the asymptotic attractor corresponding to initial conditions in the neighborhood of these boundaries. Systems with multiple attractors may also exhibit "riddled basins" [3], in which case at least one of the basins of attraction has the property that any neighborhood about each point within that basin contains points belonging to another basin of attraction. Finally, there can exist an extreme type of riddled basin, the so-called intermingled basin [3], in which all basins of attraction are riddled.

Spatiotemporal systems are high-dimensional dynamical systems. One way to study such systems is to model them as ensembles of mutually interacting low-dimensional systems arranged spatially. Examples include coupled ordinary differential equations and coupled map lattices [4]. Consider a situation where individual low-dimensional elements are chaotic, and exhibit multiple attractors and fractal basin boundaries. Due to chaotic interaction, one might argue that for each individual element, the influence of all other elements can be regarded as random noise if coupling is not strong. Since noise can wipe out of the fine-scale structure of the system on a length scale determined by the coupling strength, one might expect that arbitrarily fine fractal structures of basin boundaries would be smeared out and, consequently, spatiotemporal chaotic systems may not exhibit the type of fractal basin boundaries observed commonly in low-dimensional systems [5].

In this paper, we present evidence of an extreme type of fractal basin boundary in spatiotemporal chaotic systems modeled by globally coupled, two-dimensional maps. That is, there are regions in phase space such that any neighborhood of an initial condition which asymptotes to an attractor A contains points which asymptote to an attractor B. A scaling exponent (the so-called uncertainty exponent α [1]) used to characterize such fractal basin boundaries is estimated to be near zero, indicating an extreme sensitive dependence of asymptotic attractors on initial conditions, similar to that observed in low-dimensional systems exhibiting riddled or intermingled basins. We also demonstrate that the presence of these fractal basin boundaries implies that for fixed initial conditions, arbitrarily small parameter perturbations also lead to completely different asymptotic attractors. This results in the occurrence of "riddled parameter space" [6] in spatiotemporal chaotic systems.

Our interest in systems of globally coupled maps is motivated by the fact that they are highly simplified models for spatiotemporal dynamical systems described by nonlinear partial differential equations or coupled ordinary differential equations [5,7]. We primarily investigate a system of N globally coupled Hénon maps because the Hénon map [8] is the most extensively studied low-dimensional chaotic systems. The system is given by

$$x_{n+1}(i)=a-\left[(1-\delta)x_n(i)+\frac{\delta}{N-1}\sum_{j,j\neq i}x_n(j)\right]^2+by_n(i)\ ,$$
$$y_{n+1}(i)=x_n(i)\ ,\quad i=1,\ldots,N\ , \tag{1}$$

where i denotes discrete spatial sites, n denotes discrete time, a and b are parameters of the Hénon map, and δ is a parameter specifying coupling strength between maps at different sites. For simplicity, we assume that each map couples to every other map with uniform coupling δ. To detect possible attractors and their basins at given parameter values, maximum Lyapunov exponents (λ_1) were computed for many different initial conditions. In general, $\lambda_1>0$ signifies the existence of a chaotic attractor, while $\lambda_1\leq 0$ indicates nonchaotic motion (quasiperiodic or periodic). The phase-space dimension of Eq. (1) is $2N$.

*Present address: Department of Physics and Astronomy, Department of Mathematics, and Kansas Institute for Theoretical and Computational Science, The University of Kansas, Lawrence, KS 66045.

To study such a high-dimensional system, we take an approach of choosing a two-dimensional plane among the $2N$ phase-space variables and systematically examine the type of attractors resulting from many initial conditions chosen on this plane. For convenience, we choose a plane defined by the dynamical variables $x(i)$ and $y(i)$ at site 6. Initial values of $x(6)$ and $y(6)$ are then varied systematically, while the values of $x(j)$ and $y(j)$ $(j=1,\ldots,N, j\neq 6)$ are fixed.

In the following numerical experiments, we fix $a=1.4$ and $b=0.3$, a parameter combination which is believed to yield a chaotic attractor for the single Hénon map [8]. As the coupling δ is increased from zero, three regimes of dynamic behavior exist [6]. For small δ values, maps at different sites evolve independently, and the dynamics are usually chaotic. For large δ values, strong coherence exists among maps. For moderate δ values, interesting dynamics occur in which chaotic and nonchaotic attractors coexist at given parameter values. We have fixed the number of maps N to be 10. For this choice of N, the intermediate coupling regime is given by $0.14\leq\delta\leq 0.32$ [6].

Figure 1 shows, for $\delta=0.245$, a histogram of λ_1 values resulting from a grid of 200×200 initial conditions chosen in the two-dimensional region $-2\leq x(6)\leq 2$ and $-2\leq y(6)\leq 2$. There is a positive peak at $\lambda_1\approx 0.18$, a peak at $\lambda=0$ and a negative peak at $\lambda_1\approx -0.32$, indicating the existence of a chaotic, a quasiperiodic, and a periodic attractor, respectively [9]. The basin of the chaotic attractor is shown in Fig. 2 (black dots). In Fig. 2, the blank regions indicate basins of the quasiperiodic and periodic attractors. It can be seen from Fig. 2 that basins of chaotic and nonchaotic attractors appear to be extremely intermingled. For points that lead to the chaotic attractor, there are points nearby that lead to either the quasiperiodic or periodic attractor. This behavior persists on much smaller scales, and the fractions of initial conditions that lead to these attractors are invariant when we examine smaller and smaller scales [6]. These features thus strongly suggest that the basin boundaries between the chaotic and nonchaotic attractors are fractal.

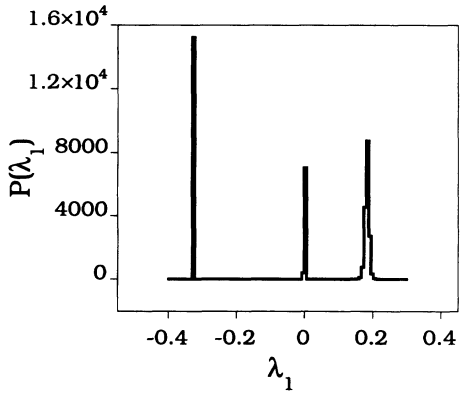

FIG. 1. A histogram of largest Lyapunov exponents λ_1 computed from 40 000 initial conditions whose $(x(6),y(6))$ values are chosen uniformly from a grid of 200×200 in $-2\leq x(6)\leq 2$ and $-2\leq y(6)\leq 2$. Three types of attractors are seen: chaotic ($\lambda_1\approx 0.18$), quasiperiodic ($\lambda_1=0$), and periodic ($\lambda_1\approx -0.32$). Parameter setting is $a=1.4$, $b=0.3$, and $\delta=0.245$ in Eq. (1).

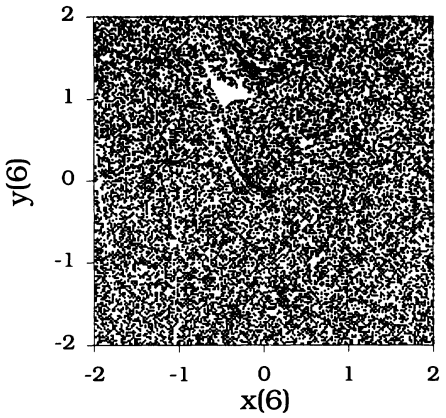

FIG. 2. The basin (black dots) of the chaotic attractor with $\lambda_1\approx 0.18$ in Fig. 1. Blank regions denote basins of the quasiperiodic and periodic attractors.

To quantify further the fractal basin boundaries, we compute the uncertainty exponent [1]. The procedure is as follows. First, we fix values of $x(j)$ and $y(j)$, for $j\neq 6$, and choose an arbitrary line segment in the $[x(6),y(6)]$ plane. Next, an initial condition with $x(6)$ and $y(6)$ values on this line segment is chosen. We then choose another initial condition on this line which is ϵ distance away from the first initial condition, where ϵ is a small perturbation, and compute λ_1 for both initial conditions. If one initial condition leads to chaos and the other gives rise to nonchaotic motion, then the first initial condition is said to be uncertain. For a given perturbation ϵ, a fraction $f(\epsilon)$ of uncertain initial conditions is obtained by randomly choosing many initial conditions on the line segment until the number of uncertain initial conditions reaches a definite large number (200 in our computation). This process is repeated for many different values of ϵ. Typically, $f(\epsilon)$ scales with ϵ as $f(\epsilon)\sim\epsilon^{\alpha}$, where the scaling exponent α is the uncertainty exponent [1]. Figure 3

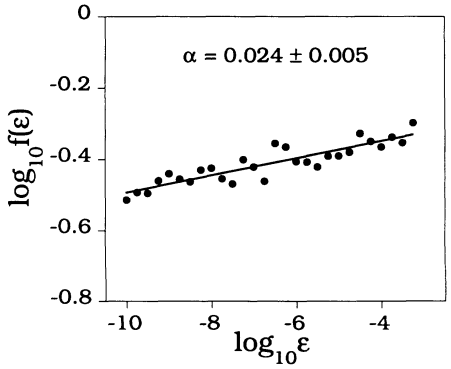

FIG. 3. Plot of the fraction of uncertain initial conditions $f(\epsilon)$ versus the uncertainty ϵ on a base-10 logarithmic scale, with the same parameter setting as in Fig. 1. The phase-space uncertainty exponent is estimated to be $\alpha=0.024\pm 0.005$.

plots $\log_{10} f(\epsilon)$ versus $\log_{10}(\epsilon)$. The slope of the fitted straight line, or an estimate of the uncertainty exponent, is 0.024 ± 0.005, a small value which is close to zero.

In numerical simulations to determine asymptotic attractors, ϵ can be viewed as the precision with which an initial condition is specified. Then the scaling exponent α determines the probability $P(\epsilon)$ that the computed asymptotic attractor is not a true one for this initial condition [1]. [Note that $f(\epsilon)$ is an approximation of $P(\epsilon)$.] If $\alpha < 1$, reduction of ϵ will result in only a small reduction of $P(\epsilon)$. In particular, in the extreme case where $\alpha \approx 0$, as shown in Fig. 3, improvement in the precision ϵ with which initial conditions are specified (even over many orders of magnitude) may result in only an incremental improvement in ability to predict the asymptotic attractor correctly. To appreciate the implication of $\alpha \approx 0$, assume that α takes its upper bound value of 0.029 in Fig. 3. Assume initial conditions can be specified to within 10^{-16}, then there is a probability of $P(\epsilon) \sim 10^{0.029(-16)} \approx 0.34$ that the final asymptotic attractor computed is incorrect. Now, suppose computer precision is improved by 16 decades to 10^{-32}. Then the probability of incorrectly computing the asymptotic attractor is $\sim 10^{0.029(-32)} \approx 0.12$, a very small improvement in uncertainty with respect to the magnitude of the improvement in computer precision [10]. This type of extreme sensitive dependence of asymptotic attractor on initial conditions is also seen in low-dimensional systems which exhibit riddled or intermingled basins [3].

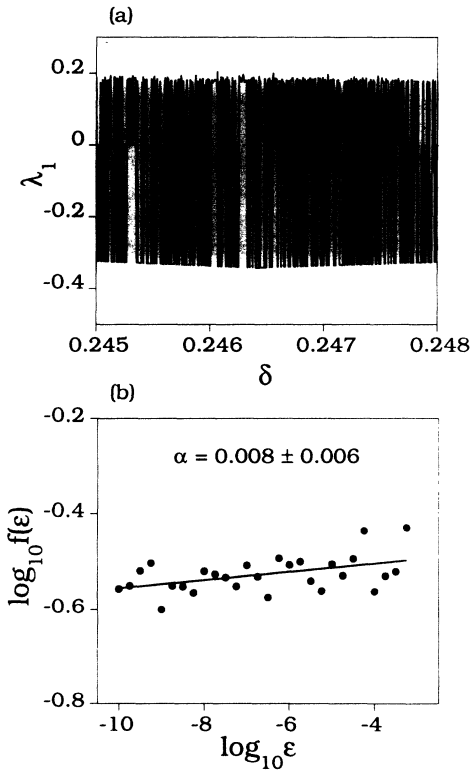

FIG. 4. (a) λ_1 versus δ for $0.245 \le \delta \le 0.248$ at fixed initial conditions; and (b) plot of the fraction of uncertain δ values $f(\epsilon)$ versus the parameter perturbation ϵ, where δ is randomly chosen in [0.14,0.32], on a base-10 logarithmic scale for $a = 1.4$ and $b = 0.3$. The parameter-space uncertainty exponent is estimated to be $\alpha = 0.008 \pm 0.006$.

The extreme type of final state sensitivity seen above may also imply a same type of dependency on parameters. Small perturbations in initial conditions at fixed parameter values may be conceptually regarded as perturbations in parameter space with fixed initial conditions. This can be seen by considering a dynamical system given by $\mathbf{x}_{n+1} = \mathbf{F}(\mathbf{x}_n, \mathbf{p})$, where $\mathbf{x}$ and $\mathbf{p}$ are phase-space variables and parameters, respectively. In the presence of a small perturbation in $\mathbf{x}_0$ that results in an initial condition $\mathbf{x}_0'$, where $|\mathbf{x}_0' - \mathbf{x}_0| \to 0$, we have

$$\mathbf{F}(\mathbf{x}_0', \mathbf{p}_0) = \mathbf{F}(\mathbf{x}_0, \mathbf{p}_0) + \mathbf{DF}_{\mathbf{x}}|_{\mathbf{x}_0, \mathbf{p}_0} \cdot (\mathbf{x}_0' - \mathbf{x}_0) \equiv \mathbf{F}(\mathbf{x}_0, \mathbf{p}_0) + \mathbf{DF}_{\mathbf{p}}|_{\mathbf{x}_0, \mathbf{p}_0} \cdot (\mathbf{p}_0' - \mathbf{p}_0) = \mathbf{F}(\mathbf{x}_0, \mathbf{p}_0') , \quad (2)$$

where $\mathbf{DF}_{\mathbf{x}}|_{\mathbf{x}_0, \mathbf{p}_0}$ and $\mathbf{DF}_{\mathbf{p}}|_{\mathbf{x}_0, \mathbf{p}_0}$ are Jacobian matrices with respect to $\mathbf{x}$ and $\mathbf{p}$, respectively. The set of parameters $\mathbf{p}_0'$ is related to $\mathbf{x}_0'$ by $\mathbf{DF}_{\mathbf{p}}|_{\mathbf{x}_0, \mathbf{p}_0} \cdot (\mathbf{p}_0' - \mathbf{p}_0) = \mathbf{DF}_{\mathbf{x}}|_{\mathbf{x}_0, \mathbf{p}_0} \cdot (\mathbf{x}_0' - \mathbf{x}_0)$. Therefore, *at fixed initial conditions,* arbitrarily small parameter perturbations may yield completely different asymptotic attractors. This is shown in Fig. 4(a), which plots λ_1 versus δ for $0.245 \le \delta \le 0.248$ at fixed initial conditions. Physically, this suggests that small perturbations in parameters alter the basin structures of different types of attractors on arbitrarily fine scales, although the overall phase-space structure remains the same. In fact, Eq. (2) implies that the uncertainty exponents computed in both phase space and parameter space should be close. This observation has been used to detect possible fractal basin boundaries in experimental settings [2]. Figure 4(b) shows $\log_{10} f(\epsilon)$ versus $\log_{10}(\epsilon)$, where ϵ is a perturbation in the parameter δ (randomly chosen from the interval [0.14,032]) for fixed initial conditions. The uncertainty exponent is estimated to be $\alpha = 0.008 \pm 0.006$, indeed a small value which is very close to zero.

Fractal basin boundaries similar to those shown above may be common in globally coupled, two-dimensional maps. We have tested Eq. (1) with N up to 80. The general finding is that these systems all exhibit the same type of phase-space and parameter-space structures [11]. The reason that fractal basin boundaries occur in spatiotemporal systems may be attributed to the complicated interaction among elements at different spatial sites as a consequence of coupling. Consequently, the mean field like coupling term in Eq. (1) behaves qualitatively differently from a random noise term, in which case the fractal phase-space structure would be destroyed. This observation is consistent with the recent results on nonstatistical properties of globally coupled maps [7]. The type of fractal basin boundaries described in this paper render unpredictable asymptotic attractors for particular initial conditions and/or parameters. This might provide insight to the fact that spatiotemporal chaotic systems are generally extremely unpredictable.

This work was supported by the National Institute of Health, Office of Naval Research, National Science Foundation, and the Whitaker Foundation.

[1] C. Grebogi, S. W. McDonald, E. Ott, and J. A. Yorke, Phys. Lett. **99A**, 415 (1983); C. Grebogi, E. Ott, and J. A. Yorke, Phys. Rev. Lett. **50**, 935 (1983); S. W. McDonald, C. Grebogi, E. Ott, and J. A. Yorke, Physica D **17**, 125 (1985); E. G. Gwinn and R. M. Westervelt, Phys. Rev. A **33**, 4143 (1986); C. Grebogi, E. Ott, and J. A. Yorke, Phys. Rev. Lett. **56**, 1011 (1986); Physica D **24**, 243 (1987); C. Grebogi, E. Kostelich, E. Ott, and J. A. Yorke, *ibid.* **25**, 347 (1987).

[2] F. C. Moon, Phys. Rev. Lett. **53**, 962 (1984); F. C. Moon and G.-X. Li, *ibid.*, **55**, 1439 (1985).

[3] J. C. Alexander, J. A. Yorke, Z. You, and I. Kan, Int. J. Bif. Chaos **2**, 795 (1992); E. Ott, J. C. Sommerer, J. C. Alexander, I. Kan, and J. A. Yorke, Phys. Rev. Lett. **71**, 4134 (1993).

[4] K. Kaneko, Prog. Theor. Phys. **72**, 480 (1984); **74**, 1033 (1985); J. P. Crutchfield and K. Kaneko, in *Directions in Chaos* (World Scientific, Singapore, 1987); Phys. Rev. Lett. **60**, 2715 (1988); K. Kaneko, Physica D **34**, 1 (1989); **37**, 60 (1989); Chaos **2**, (3) (1992), special issue on coupled map lattices, references therein, edited by K. Kaneko.

[5] D. K. Umberger, C. Grebogi, E. Ott, and B. Afeyan, Phys. Rev. A **39**, 4835 (1989).

[6] Y. C. Lai and R. L. Winslow, Phys. Rev. Lett. **72**, 1640 (1994); Physica D **74**, 353 (1994).

[7] K. Kaneko, Phys. Rev. Lett. **65**, 1391 (1990); Physica D **54**, 5 (1991); **55**, 368 (1992); S. Sinha, Phys. Rev. Lett. **69**, 3306 (1992); S. Sinha, D. Biswas, M. Azam, and S. V. Lawande, Phys. Rev. A **46**, 3193 (1992); **46**, 6242 (1992); M. Ding and L. T. Wille, Phys. Rev. E **48**, 1605 (1993).

[8] M. Hénon, Commun. Math. Phys. **50**, 69 (1976). Locally coupled Hénon map lattices have been studied by Politi and Torcini, Chaos **2**, 293 (1992).

[9] To assure that the positive peak $\lambda_1 \approx 0.18$ corresponds to a chaotic attractor rather than a long chaotic transient, we take a small grid of 32×32 initial conditions on the same two-dimensional region and evolve them under Eq. (1) for 5×10^5 iterations. It is found that the histograms obtained after 10^4 iterations are essentially the same. In particular, the number of chaotic trajectories with $\lambda_1 \approx 0.18$ does not decrease. As a further check, we take ten initial conditions that result in $\lambda_1 \approx 0.18$ at $n = 10^4$, and compute λ_1 using $n = 10^7$ interactions. The values of λ_1 obtained at $n = 10^4$ and $n = 10^7$ are the same. These tests thus suggest that the positive peak in Fig. 1 represents a chaotic attractor. On the other hand, the peaks at $\lambda_1 = 0$ and $\lambda_1 \approx -0.32$ correspond actually to quasiperiodic and periodic attractors. This is so because (1) the basins of these nonchaotic attractors contain closed regions in the phase space (Fig. 2), and (2) these zero and negative λ_1 values remain invariant as Eq. (1) is iterated in time.

[10] Near-zero uncertainty exponent means that most values of λ_1 computed are likely to be wrong, i.e., positive value could be negative. Nonetheless, the computation of the uncertainty fraction $f(\epsilon)$ and the subsequent estimation of the uncertainty exponent α are reliable. This can be argued heuristically as follows. Note that the uncertainty fraction $f(\epsilon)$ can be expressed as $f(\epsilon) = N_u / N_t = N_u / (N_u + N_c)$, where N_u is the number of uncertain parameter values, and N_c is the number of certain parameter values (parameter values that result in λ_1 with the same signs upon small perturbations). Let the uncertain probability at ϵ be p, i.e., the probability that $\lambda_1 \leq 0$ (or > 0) is p when it is numerically determined that $\lambda_1 > 0$ (or ≤ 0). The errors in N_u and N_c are thus $\Delta N_u = 2p(1-p)N_u$ and $\Delta N_c = 2p(1-p)N_c$, respectively. In other words, $\Delta N_c = \Delta N_u$, since a parameter value that is not uncertain is certain. Therefore, the error in $f(\epsilon)$ is $\Delta f(\epsilon) = (N_c \Delta N_u - N_u \Delta N_c)/(N_c + N_u)^2 = 0$.

[11] Fractal basis boundaries and near-zero uncertainty exponents not only exist for Eq. (1), which corresponds to a mean field like spatially extended system and has a translation symmetry with respect to map sites, but also exist in systems where the symmetry is broken. For example, when the parameter a is randomly chosen to be different for each map, similar fractal basin boundaries are observed [Y. C. Lai, C. Grebogi, and E. J. Kostelich (unpublished)].